30th International Congress on Sound and Vibration

ICSV30 AMSTERDAM 8-11 JULY 2024

THE INFLUENCE OF VIBRATIONS ON THE OPTIMAL PERFORMANCE OF MICRO-PERFORATED ACOUSTIC METAMATERIALS

Cédric Maury
Laboratory of Mechanics and Acoustics (LMA CNRS UMR 7031), Marseille, France
Email: cedric.maury@centrale-marseille.fr

Teresa Bravo
Spanish National Research Council, Madrid, Spain
email: teresa.bravo@csic.es

A key challenge in the building and transportation area is to enhance the acoustic absorption and insulation of porous wall-treatments over the low-mid frequency range while keeping sub-wavelength lightweight partitions. An approach is to design multi-layered thin micro-perforates with optimized constitutive parameters. However, the desired acoustic performance of the partition may often be hindered by the elasticity or the modal behavior of the thin panels. This study examines the effect of the vibrations on the sound absorption, dissipation and transmission properties of two-types of acoustic metamaterials: an acoustic fishnet made up of identical micro-perforated panels (MPP) separated by millimetric air gaps and a functionally-graded partition (FGP) composed of different MPPs with decreasing values of the holes radius across the partition. The acoustic fishnet exhibits a band gap pattern while the FGP works on impedance matching and visco-thermal dissipation through the holes as the incident wave enters the partition. Global optimization of the total power dissipated through these materials has been achieved from simulated annealing algorithm. The vibrational effects have been accounted for in an impedance translation formulation. It is found that elasticity effects broaden the first stop-band of the acoustic fishnet while lowering the dissipation peak values. They also bring added resistance to the FGP Hole-Cavity resonances that tend to merge over an extended bandwidth. The panel volumetric modes increase the absorption peaks of the acoustic fishnet if they fall just above the stop-band cut-off frequency. They also set an upper limit to the broadband properties of FGPs up to which a high dissipation, high absorption, and low transmission can be achieved. Critical coupling analysis shows how the Hole-Cavity resonances are redistributed due to coupling with the panel vibrations. It provides the amount of damping required for these resonances to achieve unit dissipation value.

Keywords: acoustic metamaterials, micro-perforates, critical coupling, vibrations, sound absorption.

1. Introduction

Designing lightweight and compact partitions able to significantly reduce the transmission of noise over a broad bandwidth or to increase its absorption is a challenging issue. It is highly relevant in the fields of aeronautical and surface transports to achieve acoustical comfort in cabins by optimizing the multi-layered structure of fuselage panels, thereby providing augmented liners with micro-perforates covering space-coiling metamaterials or dual-resonant absorbers [1]. It is also of concern in room acoustics to design quiet co-working spaces with low transmission between the individual workspaces separated from each other by, for instance, micro-perforated space sound absorbers that allow optical transparency while preventing sound transmission [2]. Even more challenging is to reduce the low-frequency components of noise disturbance that have recently emerged such as those induced by ultra-high bypass ratio fuel-efficient turbofans transmitted towards aircraft cabin [3] or the airflow noise conveyed by centralised air conditioning units towards outdoor spaces and induced by large turbines with a few number of blades [4].

Acoustic metamaterials are able to provide sub-wavelength scale solutions, in particular to achieve perfect absorption and/or blocked transmission over specific bandwidths, that can be tuned towards the low-frequency range [5]. For instance, double-layered identical perforated panels separated by a thin subwavelength air gap, have been investigated, especially the use of their Fabry-Perot Hole-Cavity resonances to block the transmission of sound under different incidence angles [6,7], the so-called double acoustic fishnet. A multi-layered acoustic fishnet has been considered with equally-spaced identical MPPs [8] to enlarge and downshift the stop-bands, although significant transmission still occurs over the first pass-band at low frequencies. This has been suppressed by shielding the device with an elastic membrane on the incident side [9]. Indeed, the large stiffness of the membrane at low frequencies blocked the sound transmission, but at the expense of large reflections.

In order to overcome this limitation and ensure both low reflection and transmission, the parameters of the multi-layered micro-perforated partitions have been optimized to maximize sound dissipation over a broad frequency range using metaheuristic algorithms [10,11] or a causal-based approach [12]. A simpler solution is to design a functionally-graded (FG) micro-perforated partition with sole monotonic axial variation of the MPP holes across the partition depth, keeping fixed the MPP and air gap parameters. This strategy leads to an interplay between impedance matching and visco-thermal dissipation at the Hole-Cavity resonances in order to achieve broadband dissipation [13]. The FG approach has also been applied to design chirped multi-layer porous materials [14]. As for micro-perforated partitions, the assumption of rigid structures is often limited by the sub-millimetric thickness of the constituting membranes [15] or by the modal behaviour of the individual plates [16]. These structural effects, such as coupling local resonators with an elastic panel, may be beneficial to broaden the efficiency range [17], but they may also be detrimental, especially if the structural and the hole-cavity resonances are strongly coupled with each other [18].

The current study examines two vibrational effects on the broadband acoustic performance of multi-layered acoustic fishnets and FG micro-perforated partitions under normal incidence: the elastic membrane and modal effects. In particular, it shows how FG micro-perforated partitions can recover high broadband dissipation performance by adding a suitable amount of damping to the panels in order to overcome the adverse effect of the panel volumetric modes. Section 2 presents the extended models used to account for elasticity and modal response of MPPs in the impedance translation approach. Section 3 examines the influence of elasticity and modal effects on the properties of multi-layered acoustic fishnets. Section 4 shows how optimized FG micro-perforated partition are influenced by these vibrational effects. It also provides a Critical-Coupling analysis of these effects and sheds light on the beneficial effect of adding a suitable amount of damping to each MPP to keep high broadband performance for the FG micro-perforated partition. Section 6 summarizes the findings and indicates follow-ups to the study.

2. Modelling the acoustic properties of multi-layered elastic MPPs

One considers a series of P MPPs, sketched in Figure 1, characterized by their thickness t_i, their holes diameter d_i and their perforation ratio $\sigma_i = \pi d_i^2/(4\Lambda_i^2)$, with Λ_i the holes pitch, separated by $(P-1)$ air layers of constant depth $D_i = D$. In case of an acoustic fishnet, the holes diameter stays constant across the partition such that $d_i = d$. As for FG micro-perforated partitions, it monotonically decreases from the front to the back panel, such that $d_{i+1} = d_i - c_i\Lambda_i/2$, $i = 1,\ldots,P-1$, with c_i the rate of decay for the holes diameter. The front panel is insonified by a normal incident plane wave and the back panel radiates a plane wave in free-field.

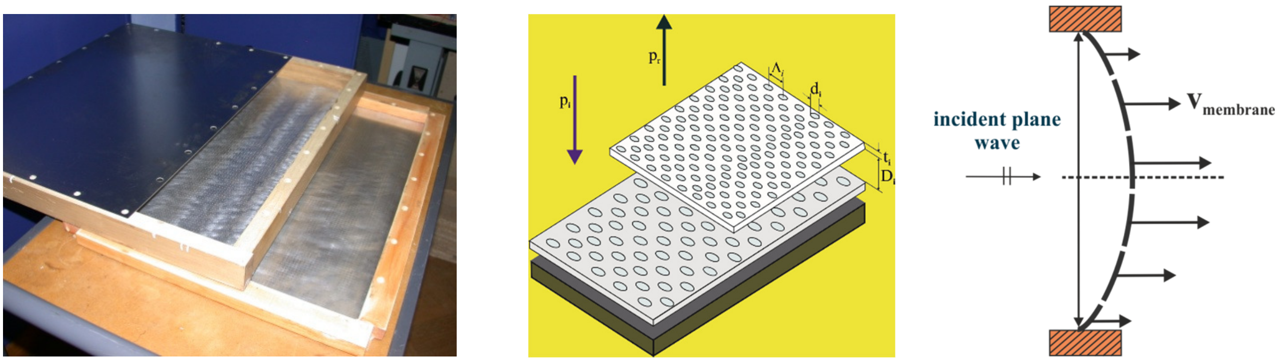

Figure 1: Picture (left) and sketch (right) of a double-layered functionally-graded micro-perforated partition; sketch (right) of the first volumetric mode of an elastic micro-perforated panel.

The overall transfer impedance of a rigid MPP, assuming zero velocity at the holes walls, is given by $Z_{\mathrm{MPP},\,i} = Z_{\mathrm{in},\,i} + Z_{\mathrm{ext},\,i}$, the sum of an inner and outer term, describing the frictional and reactive mass effects taking place respectively within and at the inlet/outlet of the MPP holes [19]. The inner transfer impedance reads $Z_{\mathrm{in},\,i} = -\mathrm{j}\omega\rho_0 t_i\left[\sigma_i\left(1 - G\left(p_i\sqrt{\mathrm{j}}\right)\right)\right]^{-1}$ where ω is the angular frequency, ρ_0 the air density, $p_i = d_i\sqrt{\omega\rho_0/(4\eta)}$ the holes perforate constant, η the air dynamic viscosity and $G(u) = 2J_1(u)/[uJ_0(u)]$ with J_1 and J_0 Bessel functions of orders 0 and 1. The outer impedance term takes the form: $Z_{\mathrm{ext},\,i} = \left[\sqrt{2}\eta\, p_i/d_i - \mathrm{j}\omega\rho_0\, 8d_i/(3\pi)\right]\ \sigma_i^{-1}$.

Assuming continuity at the in-hole walls between the air particle velocity and the MPP normal velocity, the overall transfer impedance of a thin elastic micro-perforated membrane is given by [15]

$$\tilde{Z}_{\mathrm{MPP},\,i} = \left\{\frac{1}{Z_{\mathrm{in},\,i}} + \mathrm{j}\frac{G\left(p_i\sqrt{\mathrm{j}}\right)}{\omega\rho_{\mathrm{P}}t_i}\right\}^{-1} + Z_{\mathrm{ext},\,i}\,, \tag{1}$$

with ρ_{P} the material density. The effect of the first volumetric mode of finite-sized MPPs is taken into account [16] through an extended overall transfer impedance, $\hat{Z}_{\mathrm{MPP},\,i} = Z_{\mathrm{MPP},\,i}\left(Z_{\mathrm{MPP},\,i}Y_{\mathrm{P},i} + 1\right)^{-1}$, with

$$Y_{\mathrm{P},i} = \frac{-\mathrm{j}\omega}{N_{\mathrm{P}}\rho_{\mathrm{P}}t_i}\left(\omega_{\mathrm{P}}^2 - \omega^2 - 2\mathrm{j}\xi_{\mathrm{P}}\omega_{\mathrm{P}}\omega\right)^{-1}\ , \tag{2}$$

where ω_P is the angular resonance frequency of the panel first mode, ξ_P its damping ratio and N_P the squared norm of the mode.

Applying continuity of the acoustic pressure and particle velocity at the interfaces between each MPP and the surrounding fluid domain, one gets a recursive relationship for the effective input impedance of each panel-cavity layer, $Z_{\mathrm{input},i}$ ($i=1,\ldots,P-1$):

$$Z_{\mathrm{input},i} = Z_{\mathrm{MPP},i} + Z_0 \frac{Z_{\mathrm{input},i+1}\cos(k_0 D) + \mathrm{j}Z_0 \sin(k_0 D)}{Z_0 \cos(k_0 D) + \mathrm{j}Z_{\mathrm{input},i+1}\sin(k_0 D)}, \tag{3}$$

with $k_0 = \omega/c_0$ the acoustic wavenumber, c_0 the sound speed, $Z_0 = \rho_0 c_0$ and $Z_{\mathrm{input},P} = Z_{\mathrm{MPP},P} + Z_0$ the effective impedance of the transmitting back panel. From Eq. (3), one gets the normal incidence reflection coefficient of the partition as $r = \left|(Z_{\mathrm{input},1} - Z_0)/(Z_{\mathrm{input},1} + Z_0)\right|^2$. Part of the incident power dissipated by the partition is given by $\eta = 1 - r - \tau$. τ is the transmitted power that reads $\left|2Z_{P1}/(Z_{\mathrm{input},1} + Z_0)\right|^2$ with

$$Z_{P1} = Z_0 \prod_{i=1}^{P} \frac{Z_0}{Z_0 \cos(k_0 D) + \mathrm{j}Z_{\mathrm{input},i+1}\sin(k_0 D)}. \tag{4}$$

The TL is then defined as $-20\log_{10}(\tau)$.

3. Vibrational effects on micro-perforated acoustic fishnets

The dissipation, reflection and transmission coefficients of an acoustic fishnet made up of $P = 8$ identical MPPs with thickness 0.5 mm, holes diameter 0.5 mm, perforation ratio 7.9 % and separated by an air gap of width $D = 10$ mm are simulated using the impedance translation method. Figure 2 shows the effect of assuming either elastic limp micro-perforated membranes with density 160 kg/m^3 and rectangular vibrating MPPs made in aluminium and clamped along their edge. The MPPs first volumetric mode occurs at a resonance frequency of 600 Hz and the panel damping ratio is taken as $\xi_\mathrm{P} = 1\%$.

Figure 2 shows that the acoustic fishnet exhibits a pass-band up to 2400 Hz followed by a stop band with blocked transmission and full reflection. The pass-band is populated with dissipation and transmission peaks as well as reflection dips. They occur at the Hole-Cavity resonance frequencies of the acoustic fishnet. Compared to the rigid case, it can be seen that the acoustic fishnet made up of elastic limp membranes increases the dissipation peaks and dips resulting in a uniformly damped transmission coefficient and lower values of the reflected power. This beneficial effect is due to the inertial membrane impedance factor that appears in Eq.(1), $-\mathrm{j}\omega\rho_\mathrm{P} t_i$, which brings added overall resistance to each micro-perforated membrane, thereby tending to broaden and merge the individual Hole-Cavity resonances.

Assuming vibrating MPPs, it is found that their first volumetric structural mode, localised by a red circle in figure 2, strongly perturbs the distribution of acoustical modes around 600 Hz. It induces a dissipation peak at 600 Hz preceded by a reflection peak and a null transmission at 570 Hz. This structural resonance, highly excited by the normal incident wave, falls within the half-bandwidths of the first Hole-Cavity acoustical resonances distributed over the pass-band and strongly couples with them. It downshifts the neighbouring resonances located below 600 Hz and upshifts those located above 600 Hz. The panel modal admittance given by Eq. (2) increases (resp. lowers) the effective resistance of the acoustic fishnet below (resp. above) 600 Hz, especially at the Hole-Cavity resonances. Overall, it reduces the partition transmission coefficient below ω_P but produces higher transmission above ω_P, so that the design of an insulating acoustic fishnet requires an upshift of ω_P, i.e. smaller or stiffer panels.

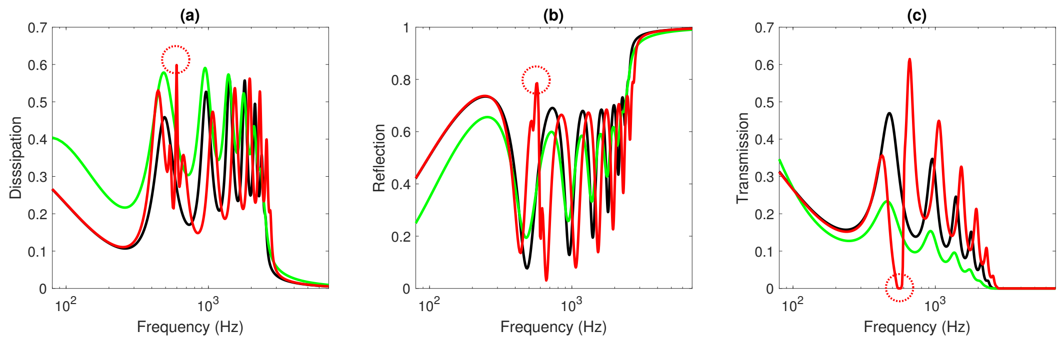

Figure 2: Influence of vibrational effects on the dissipation (a), reflection (b) and transmission (c) spectra of an acoustic fishnet made up of 8 identical MPPs assuming rigid (black), infinite elastic (green) and finite vibrating (red) panels, calculated by the impedance translation approach; the red circle shows the effect of the first volumetric mode of the vibrating panel.

4. Vibrational effects on functionally-graded micro-perforated partitions

In order to achieve both impedance matching and substantial visco-thermal dissipation of the incident wave as it enters the multi-layered partition through the MPP holes, the decay rate, c_i, of the MPP holes diameter has been optimized from simulated annealing algorithm to maximize the dissipation between 100 Hz and 1 kHz. Figure 4 shows that an almost linear decay of the holes diameter down to 0.1 mm leads to a FG micro-perforated partition whose Hole-Cavity resonances are suitably grouped and merged to achieve high dissipation (above 0.95), high TL (above 20 dB) and minute reflection (below 0.1) over the targeted frequency range, as long as rigid or limp membranes are considered (black and green curves).

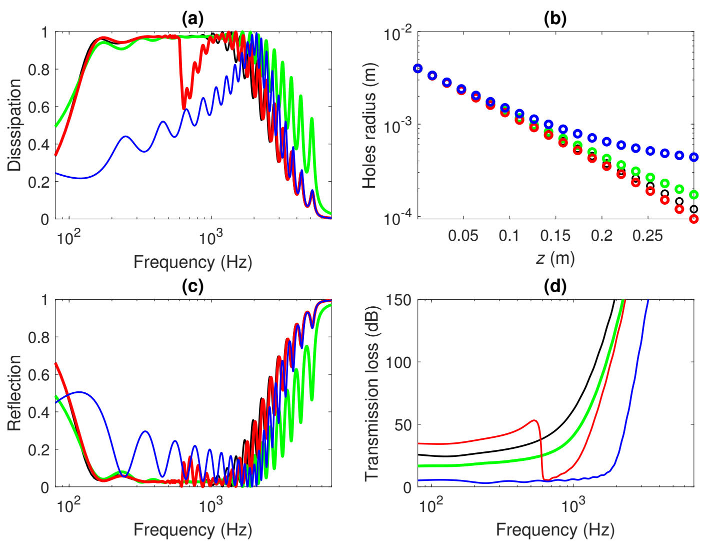

Figure 4: Influence of vibrational effects on the dissipation (a), holes radius distribution (b), reflection (c) and transmission loss (d) of optimized functionally-graded micro-perforated partitions assuming rigid (black), infinite elastic (green) and finite vibrating (red) panels, calculated by the impedance translation approach; the blue curves show the baseline properties of a non-optimized partition assuming rigid MPPs.

Further insights are obtained from critical coupling analysis [14] of the scattering matrix that relates the outgoing and ingoing amplitudes of the two-port partitions. Perfect dissipation is achieved if the eigenvalues of the matrix are zero-valued at the same real frequency. For conciseness, only the first eigenvalue has been plotted in Figures 5-7 that show a distribution of zero-poles in the complex frequency plane (f_r, f_i). The zeros such that $f_i < 0$ (resp. $f_i > 0$) are related to over- (resp. under-) resistive resonances. It can be seen from Figures 5(a) and (b) that the optimization of the rigid FG micro-perforated partition leads to two classes of Hole-Cavity resonances: those over- (resp. under-) damped below 800 Hz (resp. above 1500 Hz). A few resonances between 800 Hz and 1500 Hz are critically-coupled and achieve total dissipation at their resonance frequency. The non-optimized rigid partition exhibits under-damped resonances with $f_i > 0$ over the whole frequency range, as seen in Figure 5(c).

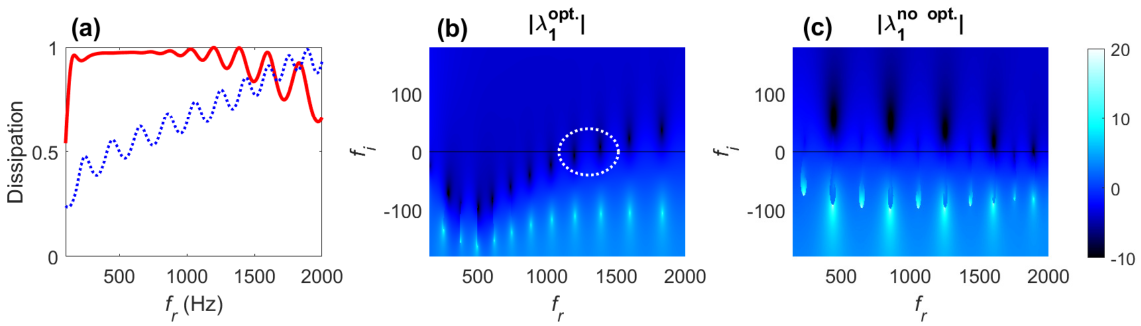

Figure 5: Dissipation spectrum (a) of a FG partition made up of rigid MPPs, whose hole diameters are optimized (plain red) or not (dotted blue), and the first eigenvalue (modulus in dB scale) of the partition scattering matrix for the optimized (b) or baseline (c) configurations; white ellipse in (b) shows the critically-coupled Hole-Cavity resonances.

Figures 6(a) and (b) show that optimizing a partition made up of elastic limp membranes further broadens the bandwidth of the over-resistive resonances up to 1200 Hz due to added overall resistance brought by the inertial membrane. It upshifts the critically-coupled resonances between 1.5 and 2 kHz.

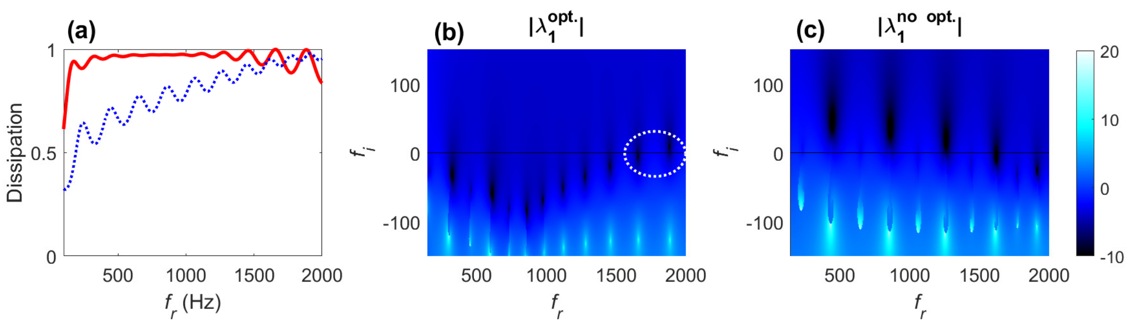

Figure 6: Effect of elasticity on the dissipation spectrum (a) (plain red: optimized; dotted blue: baseline) of a FG micro-perforated partition and on the first eigenvalue (modulus in dB scale) of the partition scattering matrix for the optimized (b) and baseline (c) configurations; white ellipse in (b) shows the critically-coupled Hole-Cavity resonances.

Figure 4 shows that optimization of the FG micro-perforated partition assuming a vibrational behaviour of each panel on its first volumetric mode (here resonant at 600 Hz) significantly reduces the bandwidth for high dissipation and high TL up to ω_P, the panel volumetric resonance frequency. Just above ω_P, one observes a substantial drop in dissipation (down to 0.6) and TL (down to 5 dB) with increase of the back-reflections up to 20%. Comparing Figure 7(b) with 5(b) indicates a significant redistribution of the zero-pole pairs in the complex frequency plane due to strong coupling between the panels' volumetric mode and the neighbouring Hole-Cavity resonances leading to multi-resonance splitting. One also observes in Figure 7(b) an accumulation of over-damped Panel-Hole-Cavity resonances as from 400 Hz that tend to be critically-coupled as their resonance frequencies approaches the panels volumetric resonance at 600 Hz. Above 600 Hz, one finds an even distribution of zero-pole pairs associated with under-damped Hole-Cavity resonances. Of interest is that one can prevent the dissipation and TL drop just above 600 Hz by increasing the panels damping ratio up to 5%, as seen in Figures 7 (a) and (c), for instance by use of viscoelastic MPPs. A suitable amount of damping downshifts the whole set of zero-pole pairs below the real axis, thereby leading to over-damped resonances, still able to group and merge up to 1 kHz. Adding further damping would lead to an overall decay of the dissipation plateau.

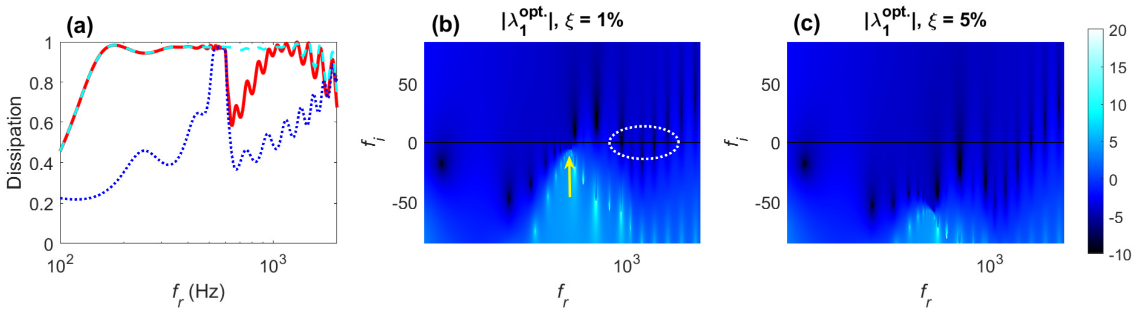

Figure 7: Influence of the first volumetric panel mode of a FG micro-perforated partition on its dissipation spectrum (a) when the dissipation is optimized (plain red: $\xi_P = 1\%$; dashed cyan, $\xi_P = 5\%$) or not (dotted blue) and on the first eigenvalue (modulus in dB scale) of the scattering matrix for the optimized partitions with damping ratios $\xi_P = 1\%$ (b) or $\xi_P = 5\%$ (c); white ellipse in (b) shows the critically-coupled Hole-Cavity resonances; yellow arrows in (b) show an accumulation of Panel-Hole-Cavity resonances below 600 Hz.

5. Conclusions

This study shows fro m the impedance translation approach and critical coupling analysis how the Fabry-Perot Hole-Cavity resonances of multilayered MPP partitions may be enhanced or hindered by vibrational effects. Elastic limp micro-perforated membranes increase the dissipation and TL of acoustic fishnets and FG partitions, but this design cannot sustain severe environments. Clamped MPP partitions provide a more robust configuration, but their optimized performance is upper limited by the resonance frequency of their first volumetric mode. This can however be overcome by adding the required amount of damping to enable merging of the Panel-Hole-Cavity resonances over a broad frequency range. Further studies should examine the optimal amount of damping required and how vibrational effects are influenced by oblique or diffuse field incidence.

6. Acknowledgments

This work is part of the project TED2021-130103B-I00, funded by MCIN/AEI/10.13039/501100011033 and the European Union "NextGenerationEU"/PRTR, and project PID2022-139414OB-I00 funded by MCIN/ AEI /10.13039/501100011033/ and by "ERDF A way of making Europe". It has also received support from the French government under the France 2030 investment plan, as part of the Initiative d'Excellence d'Aix-Marseille Université - A*MIDEX (AMX-22-RE-AB-157).

REFERENCES

1 Palma, G., Mao, H., Burghignoli, L., Göransson, P. and Iemma, U., Acoustic Metamaterials in Aeronautics, *Applied Sciences*, **8**(6), 971 (2018).

2 Sakagami, K., Toyoda, M., Yairi, M. and Okuzono, T., Three-dimensional space sound absorbers using microperforated panels, Proceedings of the *5th joint meeting of the Acoustical Society of America and the Acoustical Society of Japan*, Honolulu, Hawaii, USA, 28 November – 02 December, (2016).

3 Giesecke, D., Lehmler, M., Friedrichs, J., Blinstrub, J., Bertsch, L. and Heinze, W., Evaluation of ultra-high bypass ratio engines for an over-wing aircraft configuration. *Journal of the Global Power and Propulsion* Society, **2**, 493–515 (2018).

4 Dandsena, J., Mohapatra, K., Satapathy, A.K. and Jena, D. P., Noise control of outdoor unit of split type air-conditioner using periodic scatterers made with array of Helmholtz resonators, *Applied Acoustics*, **179**, 108054, (2021).

5 Cummer, S., Christensen, J., and Alù, A., Controlling sound with acoustic metamaterials. *Nature Reviews Materials*, **1**, 16001 (2016).

6 Christensen, J., Martinez-Moreno, L. and Garcia-Vidal, F.J., All-angle blockage of sound by an acoustic double-fishnet metamaterial. *Applied Physics Letters,* **97**, 134106 (2010).

7 Bell, J.S., Summers, I.R., Murray, A.R.J., Hendry, E., Sambles, J.R. and Hibbins, A.P., Low acoustic transmittance through a holey structure. *Physical Review B*, **85**, 214305 (2012).

8 Akozbek, N., Mattiucci, N., Bloemer, M.J., Sanghadasa, M. and D'Aguanno, G., Manipulating the extraordinary acoustic transmission through metamaterial-based acoustic band gap structures, *Applied Physics Letters*, **104**, 161906 (2014).

9 Fan, L., Chen, Z., Zhang, S.Y., Ding, J., Li, X.J. and Zhang, H., An acoustic metamaterial composed of multi-layer membrane-coated perforated plates for low-frequency sound insulation. *Applied Physics Letters,* 106, 151908 (2015).

10 Bucciarelli, F., Malfense Fierro, G.P. and Meo, M., A multilayer microperforated panel prototype for broadband sound absorption at low frequencies, *Applied Acoustics*, **146**, 134–144 (2019).

11 Shao, H., He, J., Zhu, J., Chen, G., He, H., Low-frequency sound absorption of a tunable multilayer composite structure, *Journal of Vibration and Control*, **28**, 2279–2287 (2022).

12 Bravo, T. and Maury, C., Causally-guided acoustic optimization of rigidly-backed micro-perforated partitions: Case studies and experiments. *Journal of Sound and Vibration,* **523**, 116735 (2022).

13 Maury, C. and Bravo, T., Vibrational effects of the acoustic performance of multi-layered micro-perforated metamaterials, *Vibration*, **6**, 695–714 (2023).

14 Jiménez, N., Romero-García, V., Cebrecos, A., Picó, R., Sánchez Morcillos, V.J. and García-Raffi, L.M., Broadband quasi perfect absorption using chirped multi-layer porous materials. *Advances In Physics,* **6**, 121605 (2016).

15 Li, C., Cazzolato, B. and Zander, A., Acoustic impedance of micro perforated membranes: Velocity continuity condition at the perforation boundary, *Journal of the Acoustical Society of America,* 139, 93–103 (2016).

16 Ren, S.W., Van Belle, L., Claeys, C., Xin, F.X., Lu, T.J., Deckers, E. and Desmet, W., Improvement of the sound absorption of flexible micro-perforated panels by local resonances. *Mechanical Systems and Signal Processing,* **117**, 138–156 (2019).

17 Zhang, Y., Wang, G., Zhu, Z. and Liu, Q., Vibro-acoustic coupling characteristics of the microperforated panel with local resonators, *International Journal of Mechanical Sciences*, **245**, 128125 (2023).

18 Bravo, T., Maury, C. and Pinhede, C., Enhancing sound absorption and transmission through flexible multi-layer micro-perforated structures. *Journal of the Acoustical Society of America,* **134**, 3363–3373 (2013).

19 Maa, D.Y., Potential of microperforated panel absorber. *Journal of the Acoustical Society of America,* **104**, 2861–2866 (1998).